Chapter 4

Far-field bistatic scattering simulation for rice crop biophysical parameters retrieval using modified radiative transfer model at X and C bands

4.1 Introduction

In microwave remote sensing, modeling radar responses from the target using bistatic configurations, experiment designing, and validation are active areas of scientific interest. The concept of far-field bistatic radar systems is an emerging technique with various advantages over the monostatic approach. Bistatic measurements can obtain stronger scattered echoes from the target, allow a higher system design flexibility, and provide enhanced sensitivity to temporal changes in vegetation biophysical parameters [116, 121–124]. The results of the bistatic electromagnetic model developed by [116] reported significant bistatic scattering coefficients sensitivity to vegetation biophysical parameters

in the view of obtaining higher/enhanced sensitivity. In addition, the bistatic scattering responses overcome the early saturation problem with biomass compared to the monostatic backscattering response. The term "Far-field" refers to range requirements for scattering measurement of the target by the radars. This requirement implies that the range (R) to the target must satisfy the Fraunhofer distance criterion (i.e., $R > \frac{2L^2}{\lambda}$). L is the largest lateral dimension (i.e., sidewall) of the horn aperture and λ is the wavelength used in the measurement. The Fraunhofer distance criterion can be used to find the minimum distance for optimizing the scattering responses of the intended target while maintaining maximum sensitivity. The maximum sensitivity refers to the fact that the amplitude of the scattered field may not be altered by aperture blocking, edge diffraction, and direct feed radiation [125]. The far-field bistatic radar systems are complex, require sizeable outdoor measurement, and are challenging to implement compared to monostatic radar systems [126]. It also involves synchronizing the receiver and transmitter situated at different locations.

There are only a few space-borne Earth observations satellites, namely Global Navigation Satellite System Reflectometry (GNSS-R) and TanDEM-X (an extension of TerraSAR-X mission), that work in a bistatic forward scattering alignment (FSA) convention. In the FSA convention, the polarization unit vectors (i.e., $\hat{v}$ and $\hat{h}$) are always specified to the wave propagation direction [127]. TanDEM-X is the first space-borne radar extended in bistatic FSA convention to produce a significant digital elevation model (DEM) globally [128–131]. The vegetation biophysical and land-geophysical parameters were first retrieved by GNSS-R observation over bistatic FSA convention [132–134]. Numerous advancements have been made after the European space agency (ESA) supported the companion bistatic/multistatic SAR concept, which offers an efficient and cost-effective solution when combined with the high-performing SAR mission such as Sentinel-1 [135]. Following the bistatic/multistatic companion satellite concept, ESA recently selected

Harmony for the Phase-A study of the Earth Explorer 10 mission candidate [36]. It is a concept for a bistatic companion satellite to the Sentinel-1 C band SAR instrument, which is currently developed and might be in orbit in the next 10-15 years. Therefore, it is essential to highlight the enormous potential of the bistatic concept for producing better information. The need for better information content that can shape the advancement in the future space-borne bistatic radar system could be achieved by optimizing far-field bistatic radar system in FSA convention [127, 136]. The optimum parameters selection for the far-field bistatic scatterometer measurement system in terms of frequency, polarization, incidence/scattering angle are decided based on the target scattering responses sensitivity [44].

Many theoretical studies have been reported on the polarimetric bistatic microwave scattering models, which provides insight into understanding microwave interaction with a complex medium such as vegetation, forest, snow, ocean, and bare land in remote sensing [119, 137–140]. Most of the studies are based on an approximate analytic solution to radiative transfer equation (RTE) embedded with bistatic systems geometry, frequencies, polarizations, and physical properties of the targets to determine the bistatic scattering coefficient [115, 117, 141–144]. Simulation of the bistatic scattering coefficient from various microwave scattering models facilitates the interpretation of the retrieval accuracy of physical parameters of vegetation, forest, snow, ocean, and soil with a wide range of applications.

The presented study on a radiative transfer theory-based vegetation scattering model uses an iterative approach to find scattered intensity in a specular direction to explore the insight of microwave interaction through vegetation [85, 127, 144, 145]. In the solution of RTE, the zero-order and first-order scattering (single scattering) approximations are related to the functional scattering parameterization of the water surface beneath vegetation and volume layers of vegetation. The parametric vegetation phase function (VPF) and bi-

directional reflectance distribution function (BRDF) were used to reduce the complexities of modeling scattering from vegetation volume layer and water surface beneath vegetation, respectively [67]. In addition, the first-order interaction (multiple scattering) approximations relate to the interaction of microwaves involving both surface and vegetation scattering functions [117, 127]. The parametric VPF and BRDF were optimized to the specular scattering responses measured by the far-field bistatic specular (bi-spec) scatterometer system. The simulated result enhances understanding of how frequency, angle, polarization, and design geometry affect the microwave scattering with the target properties (i.e., structural, physical, and dielectric properties). The scattering contributions (i.e., the vegetation volume layer and water surface beneath vegetation components) in the total specular scattering and retrieval of vegetation biophysical parameters were analyzed using a modified radiative transfer model (MRTM). The presented scattering model is further validated experimentally by measuring the microwave scattering response of the rice crop using an indigenous designed bi-spec scatterometer system in the FSA convention.

The present work has been divided into the following sections. Section 4.2 describes the study site and technical specification used to design a far-field bi-spec scatterometer measurement system. Section 4.3 shows the procedure for collecting in-situ vegetation observations and bi-spec scattering measurements. Section 4.4 presents the proposed methodology of the parametric bi-spec radiative transfer model. Section 4.5 shows an implementation of MRTM by empirically generated relation between vegetation optical depth (VOD) and vegetation biophysical parameters. Section 4.6 presents the simulation and retrieval performance of MRTM. Finally, Section 4.7 concludes the proposed research work.

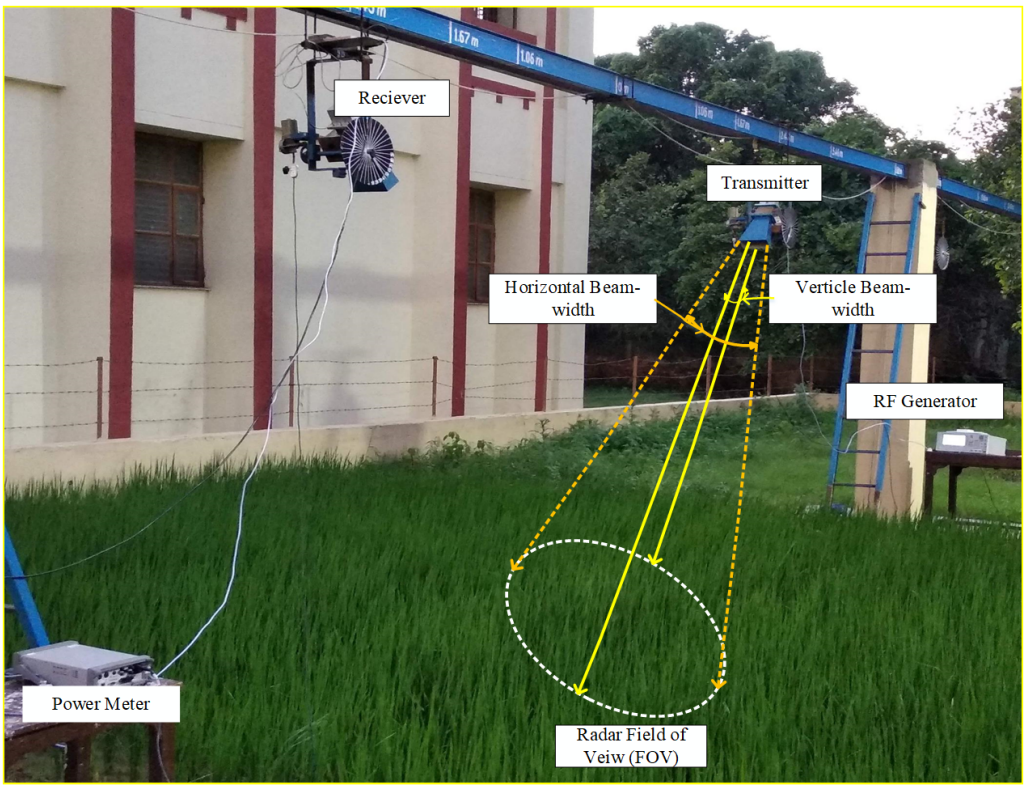

Fig. 4.1 Indigenous design of far-field bi-spec scatterometer system.

4.2 Far-field bi-spec scatterometer system

The far-field technique used for the indigenous designed bi-spec scatterometer system is shown in Figure 4.1. The bi-spec measurement was conducted on a specially prepared vegetated field of area 10m ×10m beside the department of physics, IIT (BHU), Varanasi, India. Table 4.1 indicates the technical information of the bi-spec scatterometer measurement system used in the measurement. A pair of X band ranging from 8.2 GHz to 12.4 GHz and C band ranging from 4.6 GHz to 7.05 GHz (Pasternack make) pyramidal shape horn antennas (i.e., receiving and transmitting antennas) were mounted on calibrated railing track at a height 3 meters above the ground. The pyramidal horn antenna offers a low gain variation with a nominal gain of 20 dB for X and C bands. The approximate central frequency 10 GHz (X band) and 6 GHz (C band) were used for the scattering measurement from the vegetated field. A zenith angle rotator fixed to the pyramidal horn antenna base

for its angular variation from 20° to 60° at 10° interval. No variation in azimuth direction was attempted for bistatic scattering response in this study. The power scattered from the target in a specular direction was sensed by Agilent Technologies made Average and peak power sensor (E9327A, -60 to 20 dBm, 50 MHz to 18 GHz), and measured by power meter of EPM-P series (E4416A, -70 to 44 dBm, 9 kHz to 110 GHz).

Table 4.1 Technical information of the bi-spec scatterometer system.

Parameters	Specifications	
Microwave bands	X band	C band
Range	8.2 GHz-12.4 GHz	4.6 GHz-7.05 GHz
Used frequency	10 GHz	6 GHz
Beam-width V°	16.5	16.9
Beam-width H°	16.1	14.3
Antenna type	Horn antenna	Horn antenna
Waveguide size	WR-90	WR-159
Flange size	Square Cover	Square Cover
RF generator	High power continuous wave generator (PSG) (E8257D, 10 MHz–20 GHz)	
Power meter	The power meter of the EPM-P series (E4416A, 9 kHz to 110 GHz)	
Power sensor	Average and peak power sensor (E9327A, 50 MHz–18 GHz)	
Plateform height	3-m	

4.3 In-situ measurements and data acquisition of σ^0_{pq}

The in-situ measurements of the rice crop biophysical parameters such as LAI and PWC were started after 20 days of sowing from the prepared experimental field. The sampling field conditions at various phenological stages of the rice crop are shown in Figure 4.2. The scattering response measurements were taken concurrently with in-situ LAI and PWC of the rice crop till 100 days after sowing (DAS) at 10 days intervals. Five sampling locations within the sampling field were fixed for LAI and plant height (d) measurement. A meter scale was set at five locations to measure the rice crop's plant height. The exact locations

Fig. 4.2 Sampling field conditions at various phenological stages of rice.

were used to measure LAI of different rice crop phenological stages using the LAI-2200C plant canopy analyzer (LI-COR, Inc.). The average value of five measurements was used to represent the final LAI and plant height. The destructive sampling method was opted to compute the PWC using Equation 4.1.

$$PWC = [\frac{1}{5}\sum_{i=0}^{5}(W_{Fresh\ cluster_i} - W_{Dry\ cluster_i})]\zeta \tag{4.1}$$

Where, $W_{fresh\ crop\ cluster}$ and $W_{dry\ crop\ cluster}$ represent the weight of the fresh and dry rice crop cluster, and ζ represents cluster density per square meter of rice crop within the sampling field. The weight of dry crop clusters was obtained by drying fresh crop clusters in an oven at 60°C for 72 hours.

In this experiment, the co-polarized dual polarimetric (i.e., HH and VV, where H and V represent horizontal and vertical polarization of antenna) bistatic scattering responses were measured at an approximate central frequency of X and C bands. The scatterometer measurements were performed at five specular incidence angles varying from 20° to 60° at a difference of 10°. The scattering responses of the rice crop were further used to

compute the bi-spec scattering coefficient (σ^0_{pq}) using a radar equation and expressed in dB units [146]. Where 'pq' represents the co-combination of either horizontal or vertical polarization of microwave frequency. The rice crop sampling field was flooded to a depth of around 5cm throughout the growing season at each date of radar data acquisitions to match the seasonal requirements. The calibration of the far-field bi-spec scatterometer system was made in such a way that the measured value of σ^0_{pq} from the target has been influenced by only structural properties of the target, incident/scattering angle, and frequency used in the experiment. The polarimetric bistatic calibration technique was adopted in the presented work as given in [147] and [148]. In this technique, power reflected from a large flat aluminum plate of a size compatible with the distributed target area was used to calibrate the rice crop scattering response. The far-field bi-spec scatterometer system configuration was kept the same for calibrating the target's scattering responses.

4.4 Proposed methodology

4.4.1 Problem geometry and approximation

The schematic geometrical representation of the far-field bi-spec scattering measurement system is illustrated in Figure 4.3. The narrow leaves and branches of vegetation, such as rice, wheat, etc., can be considered as disc and needle-shaped lossy dielectric vertical cylinder of uniform diameter that acts as a layer of a homogeneous medium [144, 149]. The interface between the vegetation (i.e., rice) volume layer and the water surface beneath vegetation is approximated as a structured water surface. The structured surface represents a specular water surface with scattering facets generated by the bottom of the rice crop clusters ($Z = -d$). As a result, the bottom side of each rice crop cluster within RFOV is considered to be proportional to the size of scattering facets on the structured water surface. As depicted in Figure 4.3, the polarized incident plane wave of intensity $I^i_q(\theta_d, \phi_i, 0)$

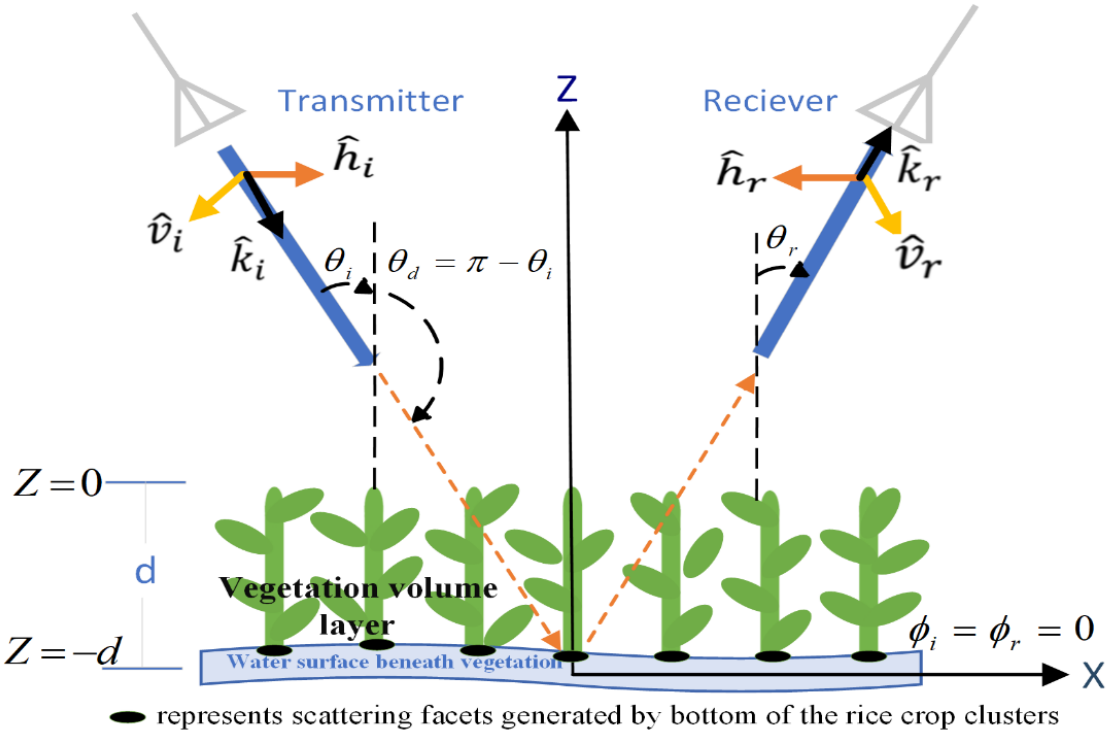

Fig. 4.3 Schematic illustration of bi-spec scattering measurement geometry.

impinges on vegetation layer and polarized scattered spherical wave of intensity $I_p^r(\theta_r, \phi_r, 0)$ from the rice crop were recorded in the specular direction at $Z = 0$. The intensity loss was neglected in the air medium present between the top of the vegetation layer and the microwave horn antennas due to the higher penetrating capability of microwave frequencies.

4.4.2 Parametric Bi-spec radiative transfer model (RTM)

The formal general solution of total upwelling and downwelling scattered radiation is generated by considering known vegetation source function as described in [127, 144] for the bistatic radiative transfer scattering model of vegetation/canopy constituent. The source function relates to the energy scattered in a specular direction due to the scattering effects from the interaction of upwelling and downwelling radiation with the vegetation constituents. However, to reduce complexity, the parametrized scattering functions such as

BRDF and VPF introduced by [68] were used to model surface and vegetation scattering. In this approach, the coupled RTE (i.e., upwelling and downwelling RTE) is transformed into parameterized integral form and solved iteratively to get zero- and first-order solutions, assuming minimal scattering albedo of vegetations volume layer [85, 94, 127, 150]. Hence, the solution to total upwelling scattered intensity in a specular direction can be represented as

$$I_q^r(\theta_r, \phi_r, 0) = I_p^{surface} + I_p^{volume} + I_p^{multiple} \tag{4.2}$$

The term $I_p^{surface}$ refers to the zero-order solution corresponding to the structured water surface beneath vegetation component attenuated by the vegetation volume layer while ignoring their scattering effects. This term plays a vital role in total scattering when scattering from the bottom of the vegetation is high, and scattering loss within the vegetation layer is negligible. The final expression of upwelling radiation scattered from the water surface beneath vegetation at $Z = 0$ is shown in Equation 4.3.

$$I_q^{surface}(\theta_r, \phi_r, 0) = I_0^i e^{\frac{-k_{ex}^- d}{\cos\theta_i}} \cos\theta_r BRDF e^{\frac{-k_{ex}^+ d}{\cos\theta_r}} \tag{4.3}$$

Where k_{ex}^+ and k_{ex}^- are upwelling and downwelling extinction coefficients, respectively. Since the scatterers are assumed to be uniformly distributed over a water surface beneath vegetation. Therefore, the extinction coefficients contribute equally (i.e., $k_{ex}^- = k_{ex}^+$) for both downwelling (θ_d) and upwelling (θ_r) directions. The direct vegetation layer's scattering contribution dominates the total scattering when VOD and scattering albedo of the vegetation layer are high. Equation 4.4 shows the expression of first-order (i.e., single scattering) solution from the vegetation volume layer at $Z = 0$.

$$I_q^{volume}(\theta_r, \phi_r, 0) = I_0^i \frac{k_s \sec\theta_r}{k_{ex}^- \sec\theta_i + k_{ex}^+ \sec\theta_r} VPF\left(1 - e^{\frac{-k_{ex}^- d}{\cos\theta_i} - \frac{-k_{ex}^+ d}{\cos\theta_r}}\right) \tag{4.4}$$

Where k_s is scattering coefficient of the vegetation volume layer. The term $I_p^{multiple}$ in Equation 4.2 refers to the first-order interaction (i.e., multiple-scattering) solution corresponding to the surface-volume, volume-surface, and surface-volume-surface components. The early stages of rice crop (approximately up to the tillering stage) have minimal scattering and absorption loss of the electromagnetic signal leading to the insignificant contribution of multiple-scattering components in the total scattered intensity. It causes the total scattered intensity to be mainly influenced by the water surface beneath the vegetation component. However, after tillering stage of the rice crop, the scattering albedo and VOD of the vegetation medium increases, resulting in higher attenuation and depolarization of electromagnetic signals. Hence, the receiver's antenna in the specular direction might experience the least intensity of multiple-scattering components. The above claim might not necessarily be valid because an increase in the scattering albedo might increase the amplitude of the first order-interaction contribution compared to the surface and canopy contribution in the specular direction. The contribution of the first-order multiple-scattering effects due to the surface-volume, volume-surface, and surface-volume-surface components within the bi-spec radiative transfer model solution for monitoring the entire growth cycle of the rice crop is not included in the presented study. Finally, the total value of the bi-spec scattering coefficient (σ_{pq}^0) corresponding to 'p' polarized incident plane wave and 'q' polarized scattered spherical wave illuminated from the vegetated rice field at Z=0 using the bi-spec scatterometer geometrical configuration set ($\theta_r = \theta_i, \phi_r = \phi_i = 0$) under the definition of specular scattering plane is shown in Equation 4.5 and is represented in dB.

$$\sigma_{pq}^0 = 10\log_{10}[4\pi\cos\theta_r(e^{\frac{-2\tau_{pq}}{\cos\theta_r}}\cos\theta_i BRDF + (1-e^{\frac{-2\tau_{pq}}{\cos\theta_r}})\frac{w_{pq}}{2}VPF)] \tag{4.5}$$

Where $\tau_{pq} = k_{ex}^{\pm}d$ and $\omega_{pq} = \frac{k_s}{k_{ex}^{\pm}}$ are known as vegetation optical depth (VOD) and single-scattering albedo of the vegetation volume layer, respectively.

4.4.3 Parametric description of VPF and BRDF

In the presented bi-spec RTM, the complexity of modeling the scattering matrix is significantly reduced by introducing parametric VPF for the vegetation volume layer and BRDF for the structured water surface beneath vegetation. The parametric scattering Henyey–Greenstein phase function HG(g,$\Phi_{a,b}$) shown in Equation 4.6 is used to approximate the structured water surface beneath vegetation and needle-shaped vegetation structure scattering characteristics, consisting of maxima in a specular direction [151].

$$VPF(g,a,b) = HG(g,\Phi_{a,b}) = \frac{1}{4\pi}\frac{1-g^2}{(1+g^2-2g\cos\Phi)^{\frac{3}{2}}} \tag{4.6}$$

Further, the VPF is modified to approximate the scattering behavior of structured water surface beneath vegetation using a bi-spec measurement system within acceptable accuracy. The active parametric representation of BRDF is shown in Equation 4.7.

$$BRDF(S,g,a,b) = \frac{S}{N(g,a)}HG(g,\Phi_{a,b}) \tag{4.7}$$

The modified factor, i.e., $\frac{S}{N(g,a)}$ in Equation 4.7 is set to mimic angular scattering behavior from the surface within the specified range of bi-spec scatterometer measurement. Therefore, it requires a comprehensive mathematical calculation to simplify the modification factor to achieve the desired output [68].

$$\frac{S}{N(g,a)} = \frac{S}{\frac{1-g^2}{2a^2g^2}\left[\frac{(1+g^2+ag)-\sqrt{(1+g^2+2ag)(1+g^2)}}{\sqrt{(1+g^2+2ag)}}\right]} \tag{4.8}$$

The scattering angle Φ within Henyey–Greenstein phase function HG(g,$\Phi_{(a,b)}$) is generalized to represent vegetation and land anisotropy by modifying its original definition [152]. The scalar product between upwelling radiation vector ($\hat{u}$) and down-welling

radiation vector ($\hat{d}$) is shown below

$$\cos\Phi = a\cos\theta_i\cos\theta_i + b\sin\theta_i\sin\theta_i\cos(\phi_i - \phi_r) \tag{4.9}$$

Where 'a' and 'b' are the weighting parameters in the scattering angle generalization for VPF and BRDF. The scattering angle generalization function considers off-specular and land/vegetation anisotropic scattering effects in the receiver's direction. The parameter 'a' is used to control the angle dependency of scattering amplitude in a specular direction. However, the land/vegetation anisotropic scattering effect can be modeled by optimizing the value of 'b' to the temporal response of σ^0_{pq} in a particular antenna direction. The parameter 'g' represents the forward scattering distributions from specular (g=1) to isotropic (g=0). Furthermore, in the following, the parameter 'g' and weighing parameters in the scattering angle generalization for both the VPF and BRDF are assumed to obey reciprocity. Therefore, the single parameter 'g' is used as scattering directionality for the VPF and BRDF. The parameter 'S' represents nadir hemispherical reflectance. The above parametric depictions of the VPF and BRDF are based on influential factors in the value of σ^0_{pq} due to far-field bi-spec system geometry, structural/physical properties of the vegetation, and structured water surface beneath vegetation.

4.5 Empirical formulation of the parametric bi-spec RTM

The penetrating ability of microwave radiation is the key reason to study microwave scattering from vegetated land surfaces. The crop canopy structure and plant water content contribute to microwave attenuation and scattering in the receiver's direction. In general, VOD describes attenuation provided by vegetation and is also dependent on microwave frequencies [153]. Thus, the parametric RTM approach is modified by introducing an empirical frequency-specific parameter (i.e., b_1 and b_2) between VOD and vegetation's

biophysical parameters (i.e., LAI and PWC) as shown in Equations 4.10 and 4.11.

$$\tau_1 = b_1\, LAI \tag{4.10}$$

$$\tau_2 = b_2\, PWC \tag{4.11}$$

Hence, the expression of σ^0_{pq} in Equation 4.5 can be modified and rewritten in terms of LAI or PWC. The value of empirically modeled frequency-specific coefficient (i.e., b_1 or b_2) was optimized based on the experimental bi-spec far-field scatterometer observations at different microwave bands. The performance of MRTM using two different auxiliary datasets (i.e., LAI or PWC) was investigated by comparing the simulated value of σ^0_{pq} with the measured value of σ^0_{pq} using a bi-spec scatterometer measurement system.

4.5.1 MRTM algorithm Implementation

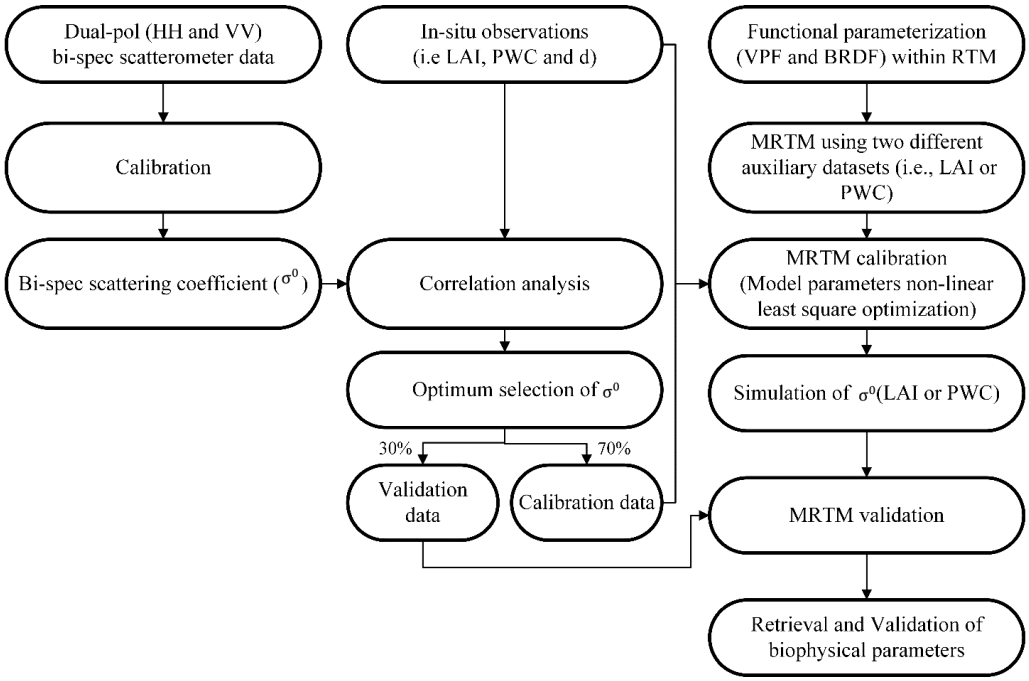

Fig. 4.4 Schematic workflow for the modified radiative transfer model-based vegetation biophysical parameters retrieval.

The overall workflow, as shown in Figure 4.4, is divided into the following steps: (1) The optimum selection of the measured σ^0_{pq} in terms of specular incidence/scattering angle, co-polarized combination, and frequencies were performed. Further, cubic spline regression was used to interpolate the optimum selection of nine-measured values of the σ^0_{pq} and in-situ biophysical parameters to generate continuous data on a daily basis. (2) Parameterization of scattering VPF and BRDF for the volume layer of vegetation and structured water surface beneath vegetation, respectively. (3) Introducing an empirical frequency-specific parameter to model temporal dynamics of the σ^0_{pq}. (4) Model parameters and an empirical frequency-specific parameter calibration by minimizing cost function using constrained non-linear least-square algorithm. (5) Comparison of performance indices on the measured and simulated value of σ^0_{pq}. (6) The retrieval performance of biophysical parameters using evolution strategies in inverse non-linear least-square optimization.

4.6 Results and Discussion

4.6.1 Assessment of in-situ biophysical parameters of the rice crop and measured σ^0_{pq} using bi-spec scatterometer measurement

The temporal response of nine in-situ d, LAI, and PWC measurements for the complete rice crop cycle at 10 days intervals from 20 DAS to 100 DAS is shown in Figure 4.5. The rice crop scattering responses were measured using a far-field bi-spec scatterometer system concurrently with in-situ biophysical parameters observation. Figure 4.6 shows temporal and multi-angular scattering response values of nine-measured σ^0 for a complete cycle of rice crop at HH and VV polarization for X and C bands. An opposite trend was observed between the measured values of σ^0 at X and C band with in-situ biophysical parameters (i.e., LAI and PWC) observation.

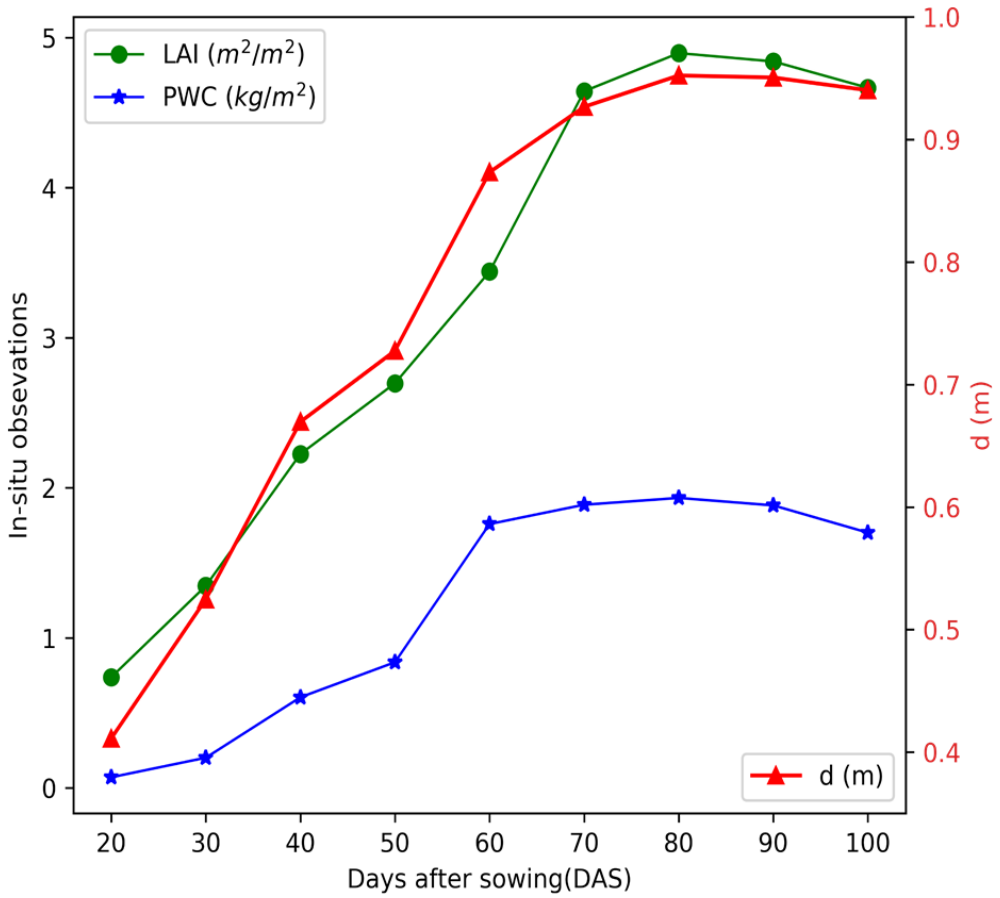

Fig. 4.5 Temporal response of in-situ observations, namely d, LAI, and PWC of rice crop.

The correlation analysis between the nine-measured values of σ^0 at X- and C band and in-situ biophysical parameters of the rice crop is summarized in Tables 4.2 and 4.3. The highly correlated value of σ^0 at different polarization combinations, incidence angles, and frequencies with in-situ biophysical parameters were considered suitable for rice crop monitoring. Hence, they were selected as an optimum combination for the indigenous-designed far-field bi-spec scatterometer system. The measured value of σ^0 was found highly correlated at 40° angles of incidence for HH and VV polarization for X and C bands. Further, cubic-spline regression analysis was carried out on the nine-measured value of σ^0 at an optimum parameter of the far-field bi-spec scatterometer measurement system and in-situ biophysical parameters to generate data daily from 20 DAS to 100 DAS.

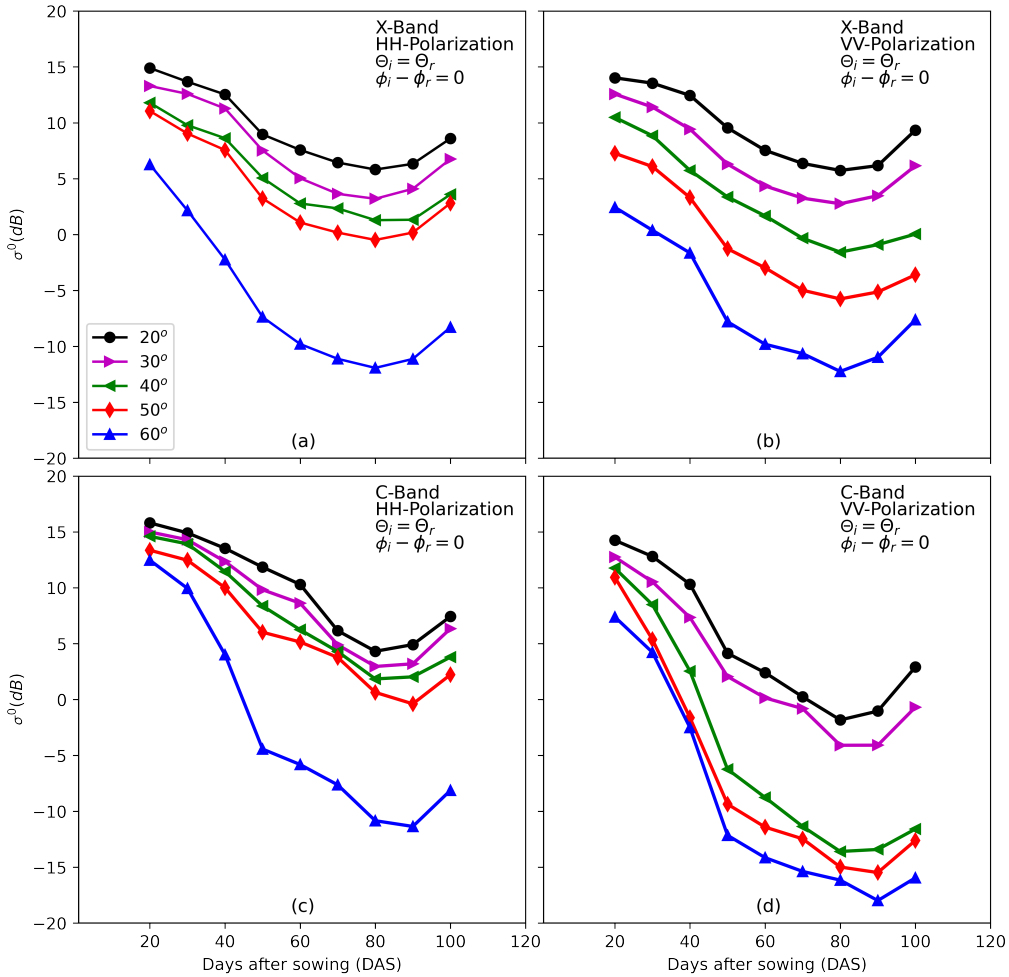

Fig. 4.6 Temporal and multi-angular scattering response value of measured σ^0 at (a) HH and (b) VV Polarization for X band; (c) HH and (d) VV Polarization for C band.

Table 4.2 The correlation coefficient between the value of σ^0 and vegetation parameters at X band.

Incidence angle (°)	Correlation (R) analysis at X band			
	HH		VV	
	LAI	PWC	LAI	PWC
20	-0.9433	-0.9615	-0.9263	-0.9578
30	-0.9371	-0.9688	-0.9337	-0.9608
40	**-0.9561**	**-0.9730**	**-0.9873**	**-0.9732**
50	-0.9369	-0.9617	-0.9700	-0.9726
60	-0.9392	-0.9497	-0.9279	-0.9509

Table 4.3 The correlation coefficient between the value of σ^0 and vegetation parameters at C band.

Incidence angle (°)	Correlation (R) analysis at C band			
	HH		VV	
	LAI	PWC	LAI	PWC
20	-0.9799	-0.9451	-0.9555	-0.9611
30	-0.9803	-0.9518	-0.9669	-0.9605
40	**-0.9877**	**-0.9711**	**-0.9700**	**-0.9633**
50	-0.9723	-0.9440	-0.9500	-0.9431
60	-0.9629	-0.9528	-0.9480	-0.9474

4.6.2 Parameters selection and inversion of MRTM

Functional parametrization

The parameters associated with the functional form of VPF and BRDF shown in Equations 4.6 and 4.7 are flexible to the geometry of the far-field bi-spec scatterometer configuration and the land/vegetation structural and physical property. The parameter 'g' of Henyey–Greenstein function is used to approximate the scattering behavior of vegetation volume layer and structured water surface beneath vegetation within VPF and BRDF, respectively. The negative values of 'g' represent the dominance of scattering in the backward direction. On the other hand, the positive values of 'g' represent the dominance of scattering in the forward direction. The magnitude of 'g' is bounded between 0 to 1. The numerical range of parameter g was temporally optimized for the entire rice crop phenology based on the measured co-polarized scattering responses at different microwave frequencies. The parameter 'a' in the scattering angle generalization for VPF and BRDF was used to approximate angular behavior in the value of σ^0. The numerical range of the parameter 'a' was selected between $0 < a < 1$, which was found plausible for the incidence angular range used in the far-field bi-spec scatterometer measurement system. The numerical value of 'a' was set at 0.5 for optimum incidence angle (i.e., 40°). The simulated value of σ^0 was found to increase with an increase in 'a' and vice versa. It

provides flexibility to simulate the temporal curve of σ^0 over wide incidence angular range used in the bi-spec scattering measurement system. The parameter 'S' represents nadir hemispherical reflectance in the BRDF and could be used to relate surface moisture beneath vegetation. The estimates of nadir hemispherical reflectance based on the optimization with experimental measurements suggest the physically plausible range as $0.1 < S < 0.3$. Hence, the chosen numerical value of 'S' was 0.2 for the theoretical simulation of σ^0 at HH and VV polarization for both X and C bands at 40° angle of incidence.

MRTM calibration Analysis

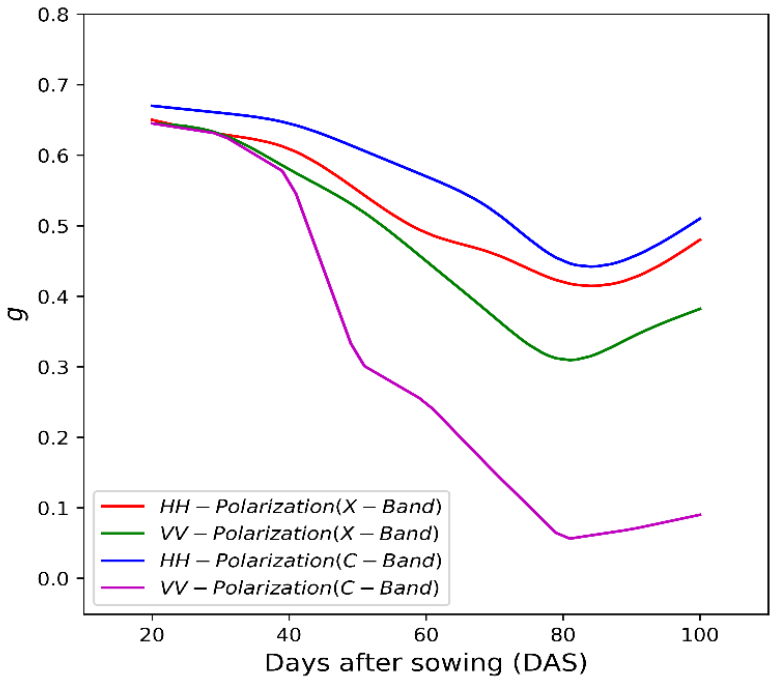

Fig. 4.7 The temporal variation of the parameter g.

A total of 81 data sets (interpolated at an interval of 1 day) comprising in-situ LAI and PWC observations along with the measured value of σ^0 at optimum parameters for the far-field bi-spec scatterometer system were divided into two sets. 70% of datasets were used to calibrate the MRTM and 30% to validate the proposed MRTM. The datasets (namely σ^0, LAI, and PWC) used in the validation of MRTM were selected at regular

intervals of 2 or 3 days to cover variability in various phenological stages of rice crop. The simulation was performed for the value of σ^0 at an optimum selection of far-field bi-spec scatterometer configuration utilizing MRTM with two different auxiliary datasets such as LAI and PWC, separately. The optimal model parameters b, b_1/b_2 and ω_{pq} were obtained by minimizing a cost function using a constrained non-linear least-square optimization algorithm.

$$cost = minimize||\sum_{i=0}^{n}(\sigma^0_{Measured_i} - \sigma^0_{Simulated_i}(LAIorPWC))^2|| \tag{4.12}$$

Where $\sigma^0_{Simulated}$ and $\sigma^0_{Measured}$ are the simulated and measured values of σ^0, respectively. Although minimizing a cost function using the non-linear least square algorithm is easy to implement, the optimization performance is significantly dependent on the favorable initial guesses with the constraints imposed on it. Hence, a priori knowledge of the model parameters and their significance is desired to calibrate the model such that the optimization process may not fall in the local minimum. The user-supplied initial guess strategy of the model parameters should be positive. The larger initial value (i.e., ≤ 2) of model parameters are avoided to neglect the unnecessary non-convexities in the problem. Based on the MRTM calibration using LAI as an auxiliary dataset, the most favorable initial ranges of the b, b_1 and ω_{pq} were found to be constrained by (1 - 1.9), (0 - 0.5) and (0 - 1), respectively. However, in the optimization process of MRTM using PWC, the most favorable initial ranges of the b, b_1 and ω_{pq} were found to be constrained by (1 - 1.9), (0 - 1.9) and (0 - 1). After optimizing model parameters, the remaining datasets were used to validate the developed MRTM.

The optimal numerical values of MRTM's parameters (i.e., b, b_1 or b_2, and ω_{pq}) in the forward simulation are depicted in Table 4.4. The high value of ω_{pq} obtained in the optimization process at HH and VV polarization for X band indicates that the vegetation scattering effects are high within the rice crop canopy. The value of ω_{pq} at VV

polarization for C band is found significantly different from HH polarization. It indicates that the vertically polarized microwave signals, with high penetrating ability, have higher absorption due to the vertical lossy dielectric stalks of the rice crop than horizontally polarized microwave signals. Furthermore, the decrease in the value of ω_{pq} for C band compared to X band demonstrates that vegetation scattering effect decreases as penetrating power of microwave frequencies increases. The frequency-specific parameter (i.e., b_1 or b_2) in the optimization was found positive, and the constraints on this parameter are dependent on the auxiliary datasets used in the MRTM. The positive value of b_1 and b_2 implies that the attenuation in the forward specular scattering is due to the vegetation scattering and absorption at HH and VV polarization for X and C bands. The temporal variation of the parameter 'g' is plotted in Figure 4.7. The decreasing trend was observed at HH polarization for X and C bands until the late dough stage of the rice crop. On the other hand, VV polarization for X and C bands showed a decreasing trend until the early dough stage reached. It is most likely due to the higher loss of vertically polarized microwave signal with the interaction of lossy vertical stalks of the rice crop than horizontally polarized microwave frequencies. The decreasing curves of parameter 'g' demonstrate that the specular scattering amplitude decreases due to the temporal change in the properties of vegetation and structured water surface beneath vegetation. In addition, the value of g > 0.6 indicates the dominance of surface scattering.

Table 4.4 The optimal numerical values of MRTM's parameters using constrained non-linear least-square algorithm.

Band-Pol	temporal range of 'g'	MRTM using LAI			MRTM using PWC		
		b	b_1	w_{pq}	b	b_1	w_{pq}
X-HH	0.6478≥g≥0.4146	1.6864	0.2508	0.7983	1.5923	0.5146	0.8984
X-VV	0.6450≥g≥0.3095	1.6510	0.2870	0.6886	1.5459	0.7201	0.7992
C-HH	0.6690≥g≥0.4420	1.7603	0.2361	0.6830	1.7078	0.4968	0.7473
C-VV	0.6435≥g≥0.0563	1.7375	0.3765	0.1035	1.6211	1.1513	0.1115

4.6.3 Analysis on specular scattering components contribution in the total value of σ^0

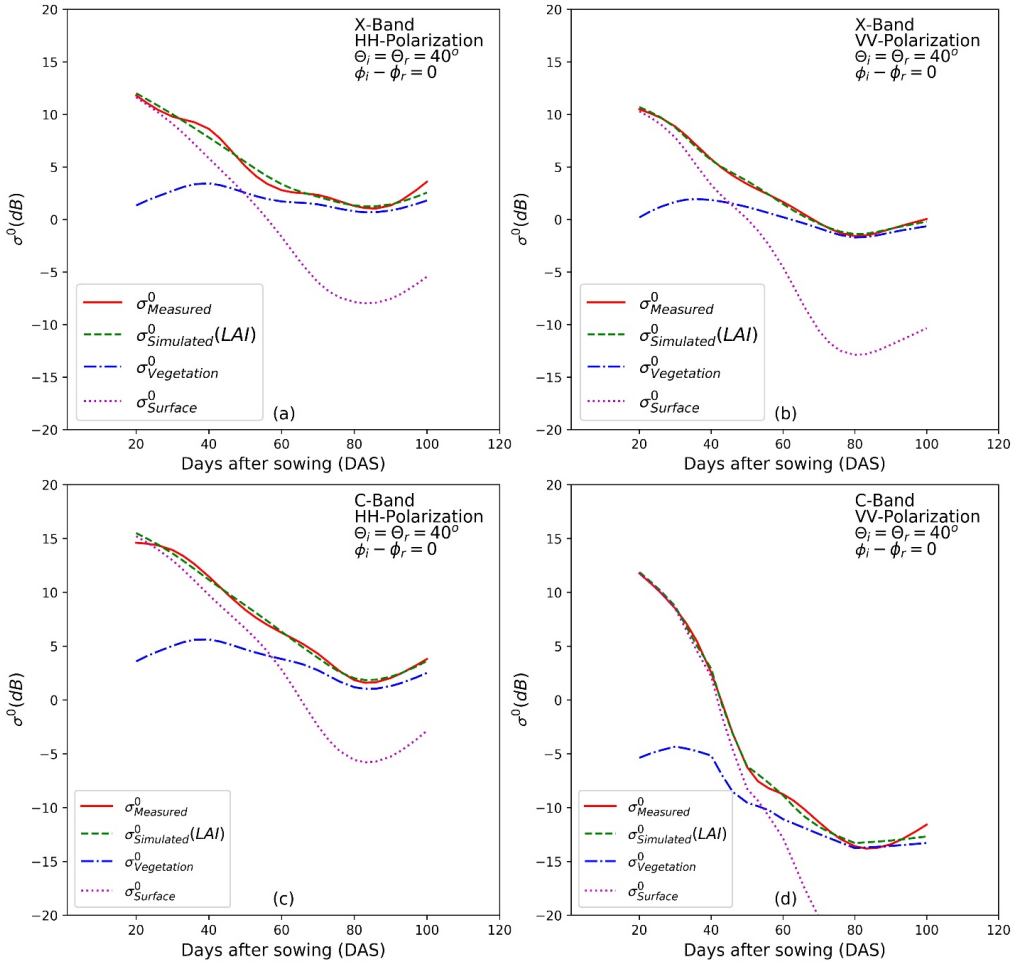

Fig. 4.8 Simulation results of MRTM using LAI at (a) HH and (b) VV Polarization for X band; (c) HH and (d) VV Polarization for C band.

The analysis was entirely based on the total specular scattering decomposition into two major specular scattering components (1) specular scattering component due to the water beneath vegetation and (2) specular scattering component due to the vegetation volume layer. Figures 4.8 and 4.9 show the simulated value of σ^0_{HH} and σ^0_{VV} at 40° angles of incidence for X and C bands utilizing MRTM with two different auxiliary datasets (i.e., LAI and PWC). The temporal variation of simulated specular scattering

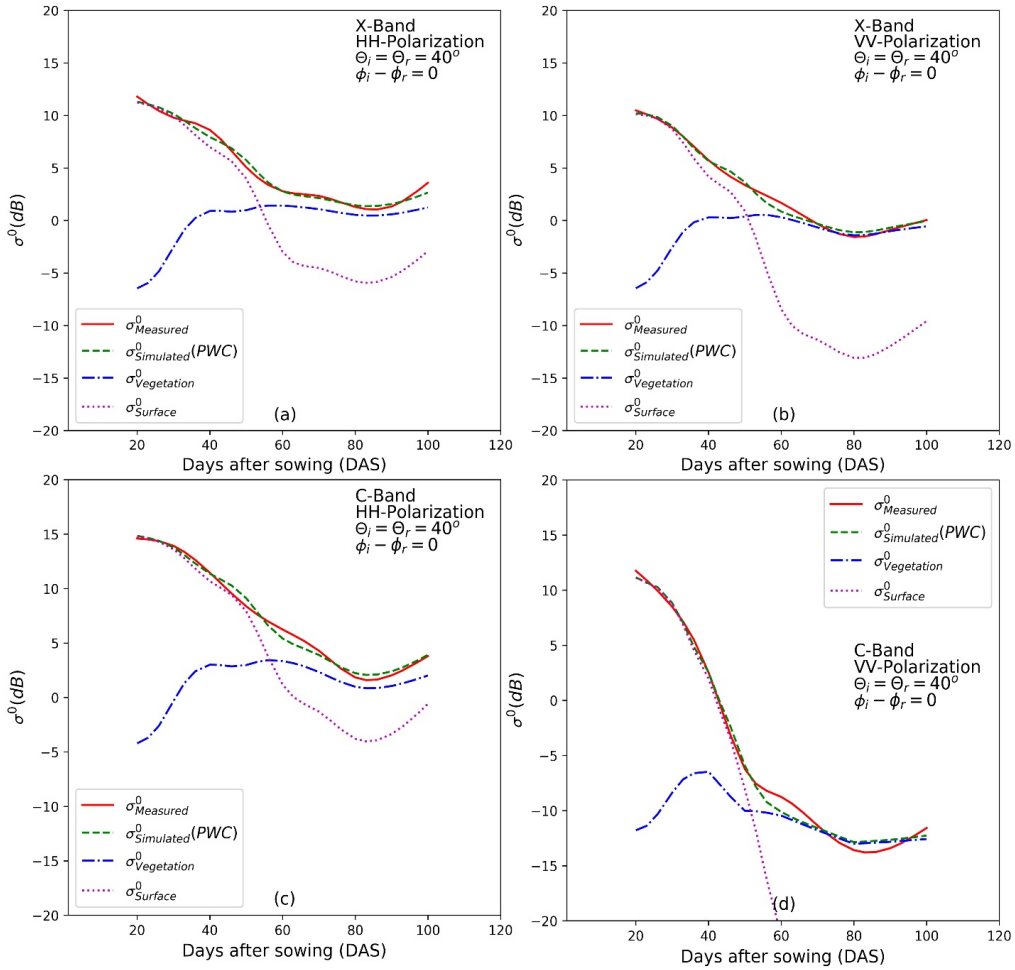

Fig. 4.9 Simulation result of MRTM using PWC at (a) HH and (b) VV Polarization for X band; (c) HH and (d) VV Polarization for C band.

components corresponding to water surface beneath vegetation and vegetation medium and their dominance in the total scattering is clearly visible in the plotted results of MRTM's. The water surface beneath vegetation contribution in the total scattering below -20dB is clipped in figures 4.8(d) and 4.9(d).

The dominance of major specular scattering components with respect to the age of rice crop was also analyzed based on the simulation results of MRTM utilizing two different auxiliary datasets (i.e., LAI and PWC). This investigation allows us to understand the insight of the temporal scattering response of σ^0 along with the change in the value of biophysical parameters of rice crop. The simulation results of MRTM using LAI

at HH and VV polarization for X and C bands are shown in Figure 4.8. The specular scattering component due to the vegetation volume layer ($\sigma^0_{Vegetation}$) starts dominating from the elongation stage (i.e., 50 DAS) of rice crop in the simulated value of total specular scattering($\sigma^0_{Simulated}(LAI)$) at HH polarization for X band. In contrast, at HH polarization for C band, the dominance of $\sigma^0_{Vegetation}$ in the value of $\sigma^0_{Simulated}(LAI)$ occurs late (i.e., from the booting stage of rice crop; 60 DAS). The reason behind the late dominance of $\sigma^0_{Vegetation}$ at HH polarization for C band compared to X band, is its higher penetrating capability. Due to the higher penetrating ability of the C band, the value of $\sigma^0_{Simulated}(LAI)$ at HH polarization was strongly dominated by the specular scattering component due to the water surface beneath vegetation ($\sigma^0_{Surface}$) till 60 DAS compared to X band. Furthermore, the simulation results at VV polarization for X band indicates that $\sigma^0_{Vegetation}$ dominates the total value of $\sigma^0_{Simulated}(LAI)$ from the late tillering stage (i.e., 46 DAS, earlier than HH polarization for X and C bands). To fully comprehend this scattering phenomenon, an investigation of the interaction of horizontal and vertical polarized microwave frequencies with the temporal change in the vertical stalk of vegetation is needed. The loss of vertically polarized microwave frequencies is significantly higher than horizontally polarized microwave frequencies due to the interaction of the vertically polarized microwave frequencies with the vertical oriented lossy dielectric stalks of rice crop. It causes a significant decrease in the value of $\sigma^0_{Surface}$ at VV polarization compared to HH polarization at X band. An early decrease in the value of $\sigma^0_{Surface}$ due to vertical stalks of rice crop at VV polarization for X band lead to the early domination $\sigma^0_{Vegetation}$ in the total value of $\sigma^0_{Simulated}(LAI)$ compared to HH polarization for X and C bands. However, due to the C bands higher penetrating power, the value of $\sigma^0_{Surface}$ at VV polarization is highly attenuated by both vertically oriented lossy dielectric cylinders (i.e., stalks of rice crop) and water surface beneath rice crop. Therefore, an abrupt decrease in the value of $\sigma^0_{Surface}$ at VV polarization for C band compared to VV polarization for X band was

found in the simulation results shown in Figures 4.8(b) and (d). As a result, the value of $\sigma^0_{Vegetation}$ at VV polarization for C band was seen dominated in the rice crop's elongation stage (i.e., 56 DAS).

The simulation results of MRTM using PWC at HH and VV polarization for X and C bands are shown in Figure 4.9. The contribution of $\sigma^0_{Surface}$ and $\sigma^0_{Vegetation}$ components in the total value of $\sigma^0_{Simulated}(PWC)$ using PWC follows a similar trend to the simulation results of MRTM using LAI. Whereas the forward shift of approximately 1 to 7 days in the dominance of $\sigma^0_{Vegetation}$ was the only significant difference observed in the simulation results of MRTM using PWC.

The value of $\sigma^0_{Simulated}$ from MRTM was experimentally validated by the value of $\sigma^0_{Measured}$ obtained by far-field bi-spec scatterometer measurements. In the forward simulation of MRTM using LAI, low root mean square error (RMSE = 0.1689) and high correlation coefficient (R = 0.9991) were computed between the values of $\sigma^0_{Measured}$ and $\sigma^0_{Simulated}$ at VV polarization for X band. However, the simulation results of MRTM using PWC showed low RMSE = 0.3814 and high R = 0.9943 at HH polarization for X band. The high accuracy between the simulated and measured value of σ^0 shows that the presented parametric approach to MRTM using both the auxiliary datasets is practical and suitable for the microwave volume scattering model using a bi-spec configuration system.

4.6.4 Retrieval of LAI and PWC

The presented parametric approach to MRTM also facilitates us to interpret retrieval of LAI and PWC from Equation 4.5 using an inverse non-linear least-square optimization algorithm. The LAI is directly correlated with the rice crop structure and foliage. Whereas the PWC is directly related to stress in crop health conditions. Therefore, LAI and PWC retrieval are important indicators for assessing and monitoring rice crop health. The 1:1 plot was drawn between the retrieved LAI and PWC with in-situ LAI and PWC to evaluate

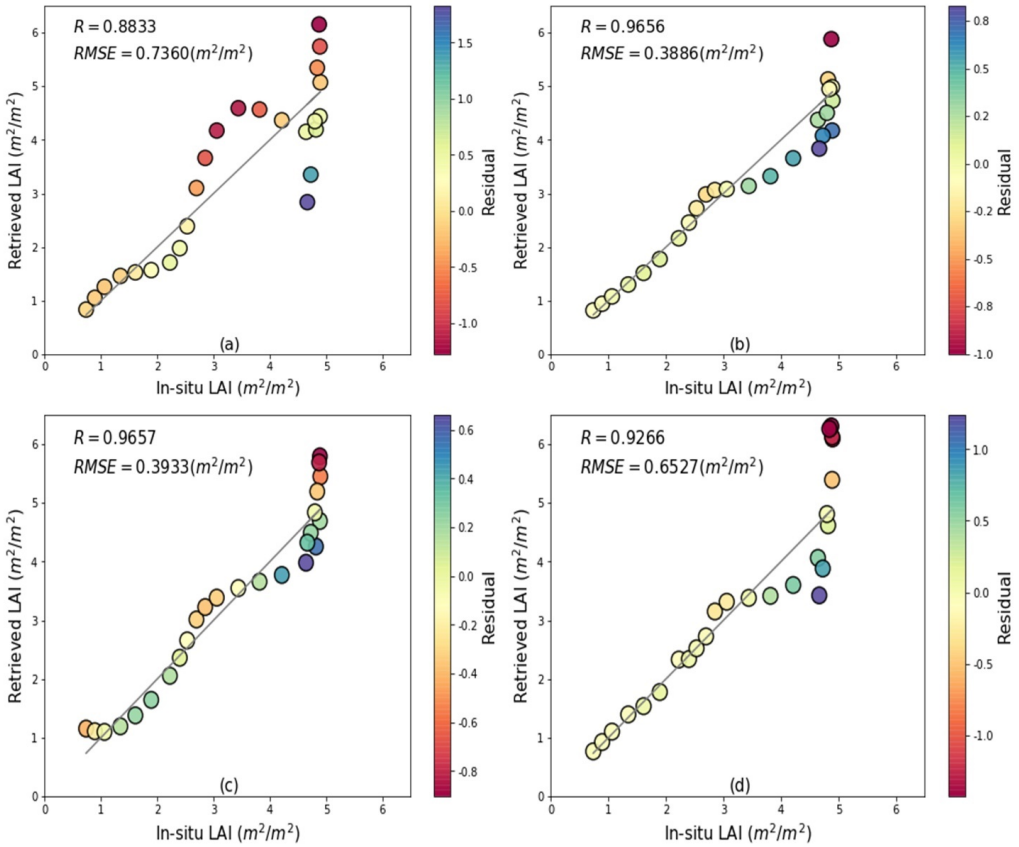

Fig. 4.10 LAI retrieval through presented MRTM using LAI at (a) HH and (b) VV Polarization for X band; (c) HH and (d) VV Polarization for C Band.

reliability at HH and VV polarizations for X and C bands in Figures 4.10 and 4.11. The LAI retrieval was best at VV polarization for X band with low RMSE= 0.3886 m^2/m^2 and high R = 0.9656 than HH polarization. In contrast, HH polarization for C band shows high LAI retrieval accuracy with RMSE= 0.3933 m^2/m^2 and R= 0.9657 compared to VV polarization. The PWC retrieval offers high accuracy with RMSE= 0.2723 kg/m^2; R= 0.9379 and RMSE= 0.2911 kg/m^2; R= 0.9359 at HH polarization for X and C bands, respectively, in comparison to VV polarization. The retrieval performance was significantly better for LAI < 4.5 and PWC < 1.5 (i.e., till vegetative growth stages of rice crop). The possible cause of poor retrieval performance during the rice crop dough stage could be the saturation of vegetative scattering with in-situ observations. Concerning retrieval accuracies, it is concluded that the proposed MRTM at X band gives promising results for

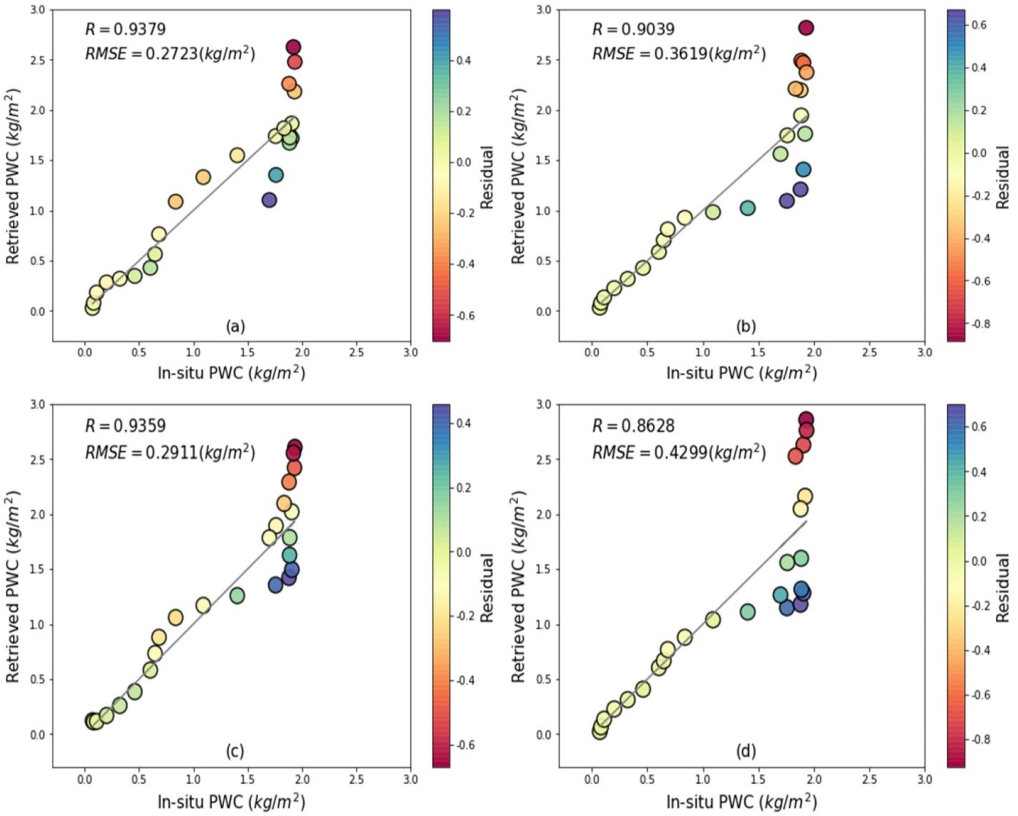

Fig. 4.11 LAI retrieval through presented MRTM using PWC at (a) HH and (b) VV Polarization for X band; (c) HH and (d) VV Polarization for C Band.

LAI retrieval at VV polarization and PWC retrieval at HH polarization at 40° angles of incidence compared to C band.

4.7 Conclusion and summary

In this study, a far-field bi-spec scatterometer system was designed in the forward scattering alignment (FSA) for observing the scattering response of the entire growth cycle of the rice crop. The scattering responses were observed at HH and VV polarization for X and C bands, which are of great interest to the microwave remote sensing community over a wide range of applications. The scattering responses observed by the far-field bi-spec scatterometer were optimized by carrying out a correlation analysis between the measured

value of σ^0 and in-situ biophysical parameters of rice crop at different combinations of specular angles, microwave frequencies, and co-polarization configurations. The measured values of σ^0 were found optimum at 40° specular incidence angle. The optimal parameters of the bi-spec scatterometer system were chosen to simulate the values of σ^0 using MRTM. Further, the values of simulated σ^0 were validated against the measured σ^0.

The parametric volume and surface scattering functions (i.e., VPF and BRDF) in the presented MRTM acts as an excellent simulator to mimic the microwave scattering response of vegetation measured by a designed far-field bi-spec scatterometer system. The parametric scattering functions in MRTM provide flexibility to analyze vegetation's scattering response over a wide zenith and azimuth angular range. Additionally, the empirical relation between VOD (i.e., τ_1 and τ_2) and vegetation biophysical parameters facilitate the MRTM to interpret the retrieval purposes. In backward modeling of MRTM, the high retrieval accuracy of LAI and PWC was found at VV and HH polarization for X band, respectively. No saturation effect was observed during the backward modeling of rice crop biophysical parameters over the entire crop cycle. However, the model performance for vegetation biophysical parameter retrieval was found poor during the dough stage of the rice crop. The retrieval of biophysical parameters from developed MRTM has excellent potential to identify different rice crop phenology at X band, leading to better options for crop health assessment and monitoring using future space-borne bistatic radar configuration.

The reported MRTM analysis is limited to only vegetation biophysical parameters sensitivity. However, the influence of land surface parameters such as soil moisture, surface roughness, and surface correlation length to the simulated values of σ^0 might also affect the retrieval accuracies of vegetation's biophysical parameters. The future studies include the following: (1) Evaluating first-order interaction components effects in the MRTM solution for the entire rice crop cycle. (2) Modifying the expression of σ^0

sensitive to both the land surface and vegetation biophysical parameters. (3) Evaluating cross-polarized sensitivity of vegetation using a far-field bi-spec scatterometer system for model validation. (4) Investigating microwave scattering phenomena for different species of cereal vegetations with reasonable computational effort, and (5) Designing a bistatic scatterometer measurement system with azimuth variation to determine the most sensitive bistatic geometric configurations for crop/vegetation growth monitoring.

****